Two-way coupled simulation of the Francis-99 hydrofoil using model order reduction

IOP Conf. Series: Journal of Physics: Conf. Series **1296** (2019) 012001 doi:10.1088/1742-6596/1296/1/012001

Two-way coupled simulation of the Francis-99 hydrofoil using model order reduction

Erik Tengs[1,2], **Johannes Einzinger**[3], **Pål-Tore Storli**[2]

[1] EDR&Medeso, Leif Tronstad Plass 3, 1337 Sandvika, Norway
[2] Norwegian University of Science and Technology, 7491 Trondheim, Norway
[3] ANSYS Germany GmbH, Staudenfeldweg 20, 83624 Otterfing, Germany

E-mail: erik.tengs@edrmedeso.com

Abstract. The Francis-99 hydrofoil is simulated using a quasi two-way Fluid-Structure Interaction procedure. The structural domain is reduced by the use of modal decomposition, and solved for inside the commercial fluid solver ANSYS CFX. Both the first order Backward Euler and second order Crank-Nicolson time discretization scheme is used in the structural equations, with significantly different results. Several coupled fluid- structure phenomena is observed that would be unobtainable in a normal one-way approach. The most interesting is an "added stiffness" effect, where the eigenfrequency of the foil increases when the flow velocity is increased. This trend corresponds well with available experimental results. The same phenomenon is observed in the hydrodynamic damping on the foil. Self-induced vibration due to vortex shedding is also simulated with good results.

The implemented two-way approach allows the different forcing terms to be tracked individually, due to the discretization of the second order structural system. This provides insight into the underlying physics behind the different FSI phenomena seen, and helps us explain why the damping and eigenfrequency characteristics change as the flow velocity passes the lock-in region.

1. Introduction

In the last couple of decades, numerical simulation and Computational Fluid Dynamics (CFD) have become one of the pillars in fluid mechanical research, alongside experiments and analytical work. The tools are in constant development and are in need of validation and testing. In the hydropower industry, the turbine designs are usually confidential, which makes it difficult for academic institutions to do research on state-of-the-art geometries. The Francis-99 workshops aims to provide an open source geometry and experimental data for validation of numerical tools and methods [1]. The model turbine is located at the Norwegian University of Science and Technology. The third Francis-99 workshop deals with Fluid-Structure Interaction (FSI). Two test cases are available to the public, one case on resonance in turbine runner channels, and one case on a more fundamental issue, hydrodynamic damping and eigenfrequencies of submerged hydrofoils. This paper will focus on the Francis-99 hydrofoil.

As part of the validation data presented for the Francis-99 Hydrofoil, two interesting figures are included and shown below, credit to Bergan et al [1, 2]. Figure 1a shows the hydrodynamic damping as a function of flow velocity. There is a distinctly different trend before and after the lock-in region. Lock-in can be defined as the frequency range where the shedding frequency of a

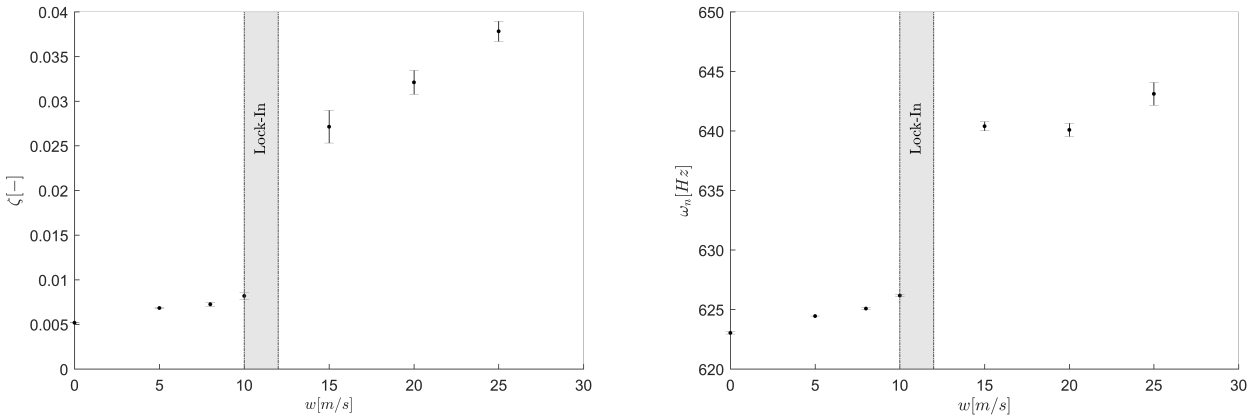

(a) Damping (b) Eigenfrequencies

Figure 1: Validation data provided by [2]

body coincide and "locks" with the natural frequency of the object in question [3]. The damping is approximately constant before, and linearly increasing, after lock-in. This experiment has been repeated with a different hydrofoil, but with the same outcome [4], and this was numerically replicated with good results [5]. This numerical work however was utilizing a one-way coupling, and although the damping was predicted, *why* the damping is different before and after lock-in was not answered in the cited works. Performing a two-way simulation may give insight into this.

The second figure, 1b, shows the natural frequency of the foil. There is a similar shifting phenomenon before and after lock-in in this case, although a linearly increasing trend after lock-in is not seen. The increase in eigenfrequency is not big, but definitely significant. Another reason why this is interesting is the fact that in a simple oscillating system, an increase in damping would correspond to a *decrease* in the eigenfrequency, not an increase. From classical structural oscillating theory we have that the damped eigenfrequency, f_d, is related to the natural frequency, f_n, in the following way; $f_d = f_n\sqrt{1-\xi^2}$, where ξ is the damping ratio [6]. Note also that the reduction in eigenfrequency should be very small, using the largest measured damping value in figure 1a, $\xi \approx 0.04$ will provide a frequency reduction of less than 1 ‰. From figure 1b we see a frequency *increase* of 30 times that. Therefore, it seems like there is an inconsistency between the the two figures and the classical theory. Or rather, that the above description of the eigenfrequency, $f_d = f_n\sqrt{1-\xi^2}$ is insufficient when the surrounding water is non-stationary. The two figures, and more importantly, the physical explanation to this behaviour, is the goal of this article. In order to obtain an understanding as general as possible, the focus will be on trends rather than obtaining the exact values.

This will be obtained by using a two-way FSI procedure. The structural problem will be reduced using a modal decomposition approach, and solved inside the fluid solver. This will provide a significant speedup compared with a traditional two-way approach, as well as a simplification of the setup.

2. Theory

The goal is to use a model order reduction scheme to reduce the structural motion such that it can be solved for inside a fluid solver. The model order reduction scheme is based on modal decomposition, and the fluid solver used is ANSYS CFX. The following sections will explain the

procedure. The two-way coupling will then be used to simulate the added mass and stiffness effects of flowing water over the Francis-99 hydrofoil.

2.1. Reduced structural model

The system we want to reduce is the usual, second order oscillating structural system [6],

$$M\ddot{u} + C\dot{u} + Ku = F \tag{1}$$

Where M, C, K, F is the mass, damping, stiffness and force coefficient matrix respectively. u denotes the deflection, and the over-dot notation indicates differentiation in time. To reduce the above equation, the principle of modal decomposition is used. For such a technique one needs the structural eigenmodes and eigenfrequencies, and thus, a modal analysis has to be performed on the system. The modal analysis, which is an eigenvalue problem, can be described as follows [7];

$$(-\omega^2 M + K)\Phi = 0 \tag{2}$$

As in all eigenproblems, the result will be the eigenvalues (ω^2) and the eigenvectors Φ_i. The scaling or length of the eigenvectors is arbitrary, however the direction is unique, and all eigenvectors are mutually orthogonal [7]. This property is used to create a modal basis Φ, a reduced vector-space, for the system. Using the modal basis, the structural deflection can be described as follows;

$$u^{n\times 1} = \Phi^{n\times m} q^{m\times 1} \tag{3}$$

The sizes of the matices/vectors are included. The superscript n denotes the degrees of freedom in the original system, and m the number of modes in the modal basis. The variable q is referred to as a modal amplitude, the scaling factor that multiplied with the mode shape results in the actual, physical deflection. If the above expression is inserted in eq 1, and then pre-multiplied with the modal basis, you get the following [8]:

$$\Phi^T M\Phi\ddot{q} + \Phi^T C\Phi\dot{q} + \Phi^T K\Phi q = \Phi^T F \tag{4}$$

Where the new, reduced coefficient matrices are of the following order, $[\Phi^T]^{n\times m} M^{n\times n}\Phi^{n\times m} = M_{red}^{m\times m}$. This illustrates the model order reduction as $m << n$.

An advantage of using the eigenmodes to create a modal basis is that due to the orthogonality of the modes, the reduced system will be diagonal, consisting of a set of linearly independent, 1-dimensional equations. This will simplify calculations, and also let us express the structural deformation as a superposition of the different structural modes, Φ_i. Note that in eq. 2, the eigenmodes were calculated without damping. To preserve the diagonal system we assume Rayleigh/ proportional damping [6].

Let the coefficients in equation 4 still be denoted M,C,K and F for simplicity. The coefficient of $\ddot{q}$ is usually normalized such that $\Phi^T M\Phi = 1$ [9]. The second order system can now be written as;

$$M\ddot{q} + C\dot{q} + Kq = F \tag{5}$$

Let the damping ratio ξ be defined as $\xi = C/(2M\omega)$ and the natural frequency $\omega = \sqrt{K/M}$, and we can derive the following [6] (recall that the matrices are diagonal);

$$\ddot{q}_i + 2\omega\xi\dot{q}_i + \omega^2 q_i = f_i \tag{6}$$

Note that the new second order harmonic system is now decoupled from the physical meaning of equation 1. Equation 6 solves for the modal displacement, using the modal force. The actual structural deformation is recovered by equation 7.

$$u = \sum_{i}^{m} \Phi_i q_i \tag{7}$$

The big advantage of the above representation, is that the solution to the structural motion is now reduced to solving a set of independent 1-dimensional equations for the modal amplitude, instead of solving for the deflection in the complete solution space.

2.2. Numerical discretization in CFX

The above section reduced the structural motion to equation 6 and 7. Further modification is needed for this to be solvable inside the commercial fluid solver ANSYS CFX. Specifically, a time discretization method is needed, the first order backward Euler and the second order Crank-Nicolson method will be presented here.

In both the discretization methods, the original second order system is split into two, first order systems, one for the displacement, and one for the velocity, illustrated below using the implicit, backward Euler scheme [10];

$$\begin{aligned} \frac{q_{i,k+1} - q_{i,k}}{\Delta t} &= v_{i,k+1} \\ \frac{v_{i,k+1} - v_{i,k}}{\Delta t} &= -2\omega\xi v_{i,k+1} - \omega^2 q_{i,k+1} + f_{i,k+1} \end{aligned} \tag{8}$$

where the subscript $i = 1, 2, ..., m$ denotes the mode, and the subscript $k = 1 \rightarrow \infty$ denotes the discretization in time. The forward Euler scheme is identical, except all (k+1) subscripts on the right-hand side is replaced with (k) only.

The Crank-Nicolson time discretization scheme is a linear combination of the forward and backward Euler method [10];

$$\begin{aligned} \frac{q_{i,k+1} - q_{i,k}}{\Delta t} &= 0.5(v_{i,k+1} + v_{i,k}) \\ \frac{v_{i,k+1} - v_{i,k}}{\Delta t} &= 0.5(-2\omega\xi v_{i,k+1} - \omega^2 q_{i,k+1} + f_{i,k+1} - 2\omega\xi v_{i,k} - \omega^2 q_{i,k} + f_{i,k}) \end{aligned} \tag{9}$$

The expression for velocity can be inserted in the expression for the acceleration, then rearranged to isolate the unknowns $q_{i,k+1}$, $v_{i,k+1}$ on the left hand side, to obtain the final Crank-Nicolson scheme:

$$\begin{aligned} q_{i,k+1} &= \frac{q_{i,k}(1 + \omega\xi\Delta t - \frac{1}{4}\omega^2\Delta t^2) + \Delta t v_{i,k} + \frac{1}{4}\Delta t^2(f_{i,k+1} + f_{i,k})}{1 + \omega\xi\Delta t + \frac{1}{4}\omega^2\Delta t^2} \\ v_{i,k+1} &= 2\frac{q_{i,k+1} - q_{i,k}}{\Delta t} - v_{i,k} \end{aligned} \tag{10}$$

The same procedure is done for the backward Euler scheme for a similar result. The final expression for $q_{i,k+1}$ consists only of known quantities, namely the eigenfrequency of that mode, the (structural) damping, the time step size, and the modal force calculated by the fluid solver at that time step. The old value of the modal amplitude, velocity and force needed to calculate

the expression is stored using a Fortran script, and called upon during calculation. The modal force has not been properly defined yet. From equation 5 to 6 the force matrix is divided by the diagonal mass matrix to obtain $f_i = F/M[\frac{N}{kg \cdot m^2}]$. The forcing is decoupled into the force projection onto the different modes and is implemented as

$$f_i = \frac{1}{M} \int_A p \cdot \Phi_i dA \tag{11}$$

where p is the fluid pressure. The above (eq. 10-11) can be implemented in CFX using the CEL expression language. The performance of the different discretization schemes will be presented in the results section.

2.3. Reduced velocity

In order to compare results across hydrofoil geometries, experiments, and simulations, it is desirable to use a different variable than the flow velocity. Bergan et al. [11] presents a reduced velocity, $v^* = v/f_n$, defined as the flow velocity divided by the eigenfrequency of the vibrating hydrofoil. In a way, this describes how much water that passes the foil during one vibrational period. It was found that if the damping was expressed with respect to v^*, then many different foils showed near identical behaviour, namely a change in damping characteristics around $v^* \approx 0.02$. This is also seen in figure 1a, as $v^* \approx 11.5/625 = 0.018$. The reduced velocity is similar to the inverse of the famous Strouhal number, $St = fL/v$, used to link the shedding frequency of vortices in the wake of an object to the flow velocity [12, 13], but without the characteristic length.

The simulations in this paper is 2D to speed up the process. As a consequence, the surface area of the foil changes compared with the 3D case. This will in turn reduce the surface force on the foil (see eq. 11), which affects the eigenfrequency. The result is as follows; in a 2D simulation, the added mass effect is smaller than in 3D, and the loaded eigenfrequency will therefore be closer to that of the foil vibrating in vacuum. By presenting the result using the reduced velocity v^* from above, the 2D simplification should not affect the results, as the flow velocity is normalized with the eigenfrequency.

3. Method

The focus have been the Francis-99 hydrofoil, more information about the hydrofoil can be found in the paper by Bergan et al, or the workshop website [1, 2]. For reference, the first bending mode (trailing edge motion) of the hydrofoil is shown in figure 2, with exaggerated deformation for illustration. Three test cases have been performed, a comparison of the discretization schemes, a simulation of self-induced vibration, and an attempt to replicate the damping and eigenfrequency behaviour across the lock-in region.

3.1. Discretization schemes

The first task is to assess the different discretization schemes. In this test case, a cantilever beam has been used for simplicity. The setup is as follows; the beam has been given an initial deflection ($\approx 3\%$ of the total length), then released. The structural damping has been set to zero, $\xi = 0$, and importantly, the fluid force (f_i in equation 6) have been hardcoded to be zero. This results in a system of equations for the structural deformation that purely consists of the structural mass and stiffness term. Theoretically, this system, given an initial deflection, should result in the following solution: $u = A \cdot cos(\omega t)$. That is, a perfect sinusoid with constant amplitude and frequency.

This test case is natural to use as it will reveal if any of the discretization schemes exhibit any unwanted *numerical* damping. The simulations were performed using 100 timesteps per oscillatory period.

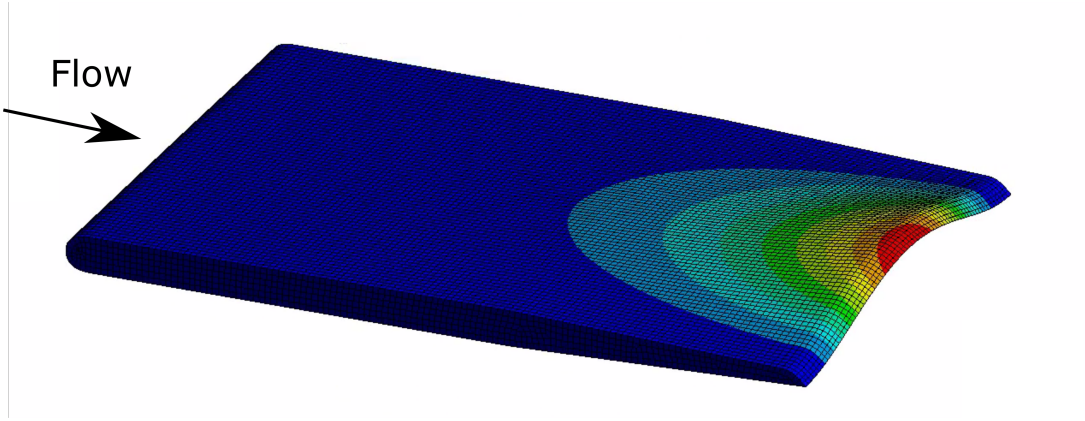

Figure 2: First bending mode of Francis-99 hydrofoil

3.2. Self-induced vibration

The coupled physics phenomenon of self-induced vibration will be simulated next. Fluid flow across an object will, at certain Reynolds numbers, induce an oscillatory pressure and velocity field. This field creates vortices trailing the body, and the body itself will experience periodic forces perpendicular to the flow direction [14]. If these periodic forces are close to the eigenfrequency of the structure, resonance can occur in the worst case. The structural vibration can also magnify the shedding of vortices and can therefore have a self-magnifying effect.

A phenomenon called "lock-in" is also something that can be observed during vortex shedding. In general, the frequency at which the vortices are shedded is linearly dependent on the flow velocity [3, 15]. If the flow velocity however, is such that the shedding frequency is close to the eigenfrequency of the structure, then the shedding frequency will "lock" to the structural frequency rather than increase linearly. For reference, Particle Image Velocimetry and CFD simulations have been used on this geometry in a previous study [16]. The simulations in that study was pure CFD, meaning no structural motion.

The hydrofoil was subjected to flow velocities in the range $v^* = [0.12 - 0.25]m$, and the SST turbulence model was used in all simulations.

3.3. Damped Vibration

The final task is to assess the added damping and stiffness effects of the flowing water. This is done by the use of damped vibration. The solution to a system of damped vibration without external forces is in the most general form the following [6];

$$x(t) = A \cdot e^{-\xi\omega t} \cdot cos(\omega_d t + \phi) \tag{12}$$

In essence, this is a sinusoid enveloped by an exponential decay. The sinusoid contains the oscillating part of the solution, i.e. the eigenfrequency, and the exponential decay contains the damping part of the solution. This representation is used when the results are analyzed.

The analysis was set up as follows; the hydrofoils was given an initial deflection, and the *structural* damping was set to $\xi = 0$. Any damping of the foil will therefore originate in hydrodynamic forces. All simulations were performed with approximately 150 timesteps per oscillatory period, and was allowed to oscillate for at least 20 periods. This ensures that the error in estimating the damping and the submerged, loaded eigenfrequency was minimized. The error in the damping was estimated to be $\approx 1.5\%$ (using a 95% confidence interval of the exponential fit), and the error in the eigenfrequency, $\approx 0.6[Hz]$.

4. Results and discussion

4.1. Discretization schemes

Figure 3 shows the normalized structural deformation of the beam using Euler and Crank-Nicolson discretization scheme. Recall that in the test of discretization schemes, the structural damping and the fluid damping is set to zero to highlight any unwanted numerical damping.

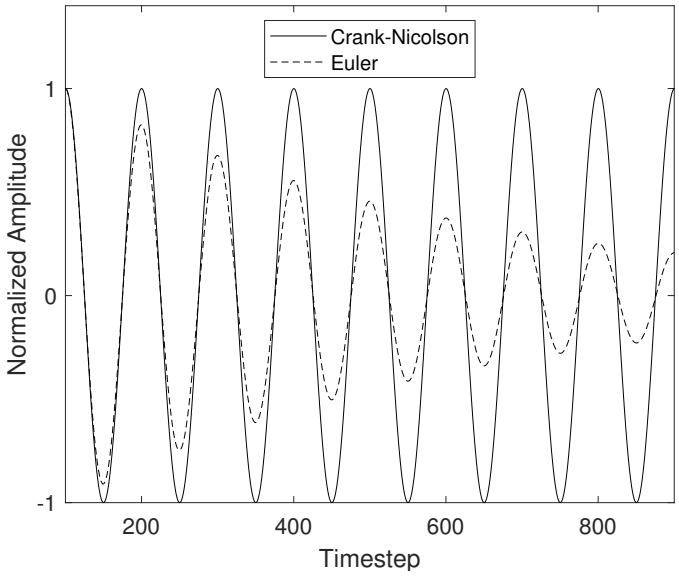

Figure 3: Comparison of the different discretization schemes

Clearly the performance of the Crank-Nicolson scheme is superior, with no numerical damping under the given conditions. The numerical damping in the Euler scheme is estimated using exponential decay to be $\approx 3\%$. This is not a large number, it is no larger than what is expected from the surrounding fluid flow [2, 17], however the effect on the displacement over time is significant. It is larger than can be accepted for subsequent simulations. The number of timesteps per period, 100, is considered sufficient and in the order of what would be used in a normal simulation. Based on the above it is therefore concluded that the Crank-Nicolson scheme should be used, especially as it carries no additional computational cost.

The Euler scheme displayed some unwanted numerical damping, compared with Crank-Nicolson. Evaluating the scheme using a Taylor expansion;

$$u_k = u_{k+1} - \Delta t \left(\frac{du}{dt}\right)_{k+1} + \frac{\Delta t^2}{2!}\left(\frac{d^2u}{dt^2}\right)_{k+1} + H.O.T. \tag{13}$$

where H.O.T denotes higher order terms. Rearranging will give the following;

$$\frac{u_{k+1} - u_k}{\Delta t} = \left(\frac{du}{dt}\right)_{k+1} - \frac{\Delta t}{2!}\left(\frac{d^2u}{dt^2}\right)_{k+1} + H.O.T. \tag{14}$$

Where we see that the scheme produces the time derivative we seek (it is *consistent*), and that the scheme is first order accurate, as predicted. Interestingly, the first order error term is related to a $\frac{d^2u}{dt^2}$ - acceleration operator. The damping seen in figure 3 is likely to originate in this term. This might indicate that structures with high eigenfrequencies, and thus high acceleration, will be more sensitive to discretization error. The structure in this case does have a fairly high eigenfrequency, however a sensitivity study on this have not been performed.

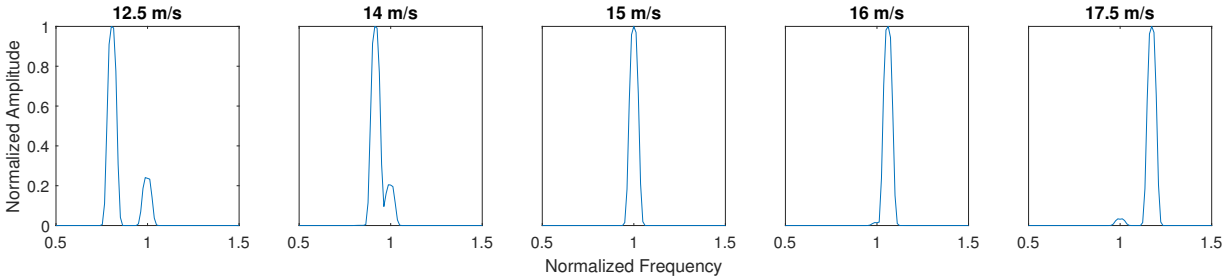

Figure 4: Frequency content during simulations of self-induced vibration

4.2. Self-induced vibration

Figure 4 shows the frequency spectrum of the vibration of the hydrofoil. The magnitude is normalized such that the different flow velocities can be compared. Interestingly, we see a component of the structural eigenfrequency ($f = 1$ in the figure) in all the simulations, along with another frequency component. The other component is the shedding frequency.

Figure 5 shows on the left axis the dominating frequency component as a function of the reduced velocity. The relation is close to linear as expected, however there is some discrepancy around the point where the eigenfrequency of the foil matches the shedding. This is signs of the lock-in phenomenon, although not as clear as was shown in other experimental works [16, 3]. On the right axis, the normalized amplitude of the self-induced vibration is plotted. It is clear that the effect of resonance is extreme.

Another finding is that the reduced velocity at which these phenomena occur is exactly where Bergan et. al [11] predicted, $v^* \approx 0.018 - 0.02$, even though this is a 2D representation of the foil, with changed eigenfrequency. This is a great justification of the use of the reduced velocity.

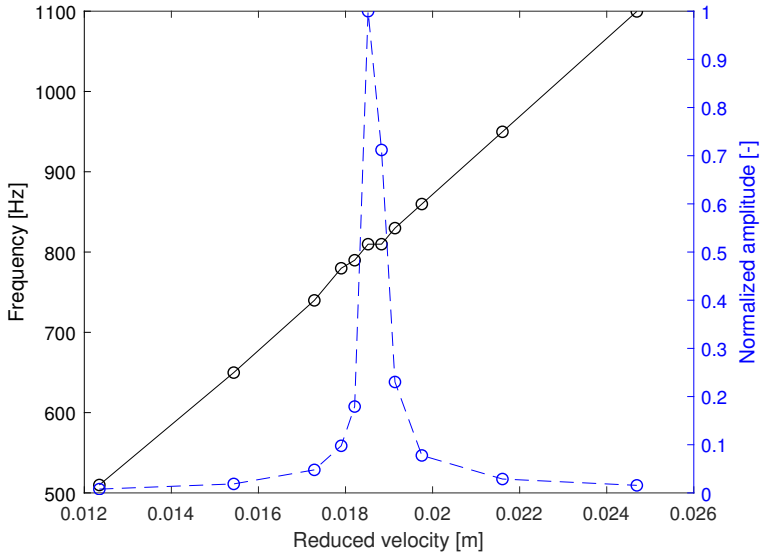

Figure 5: Shedding frequency and lock-in effect

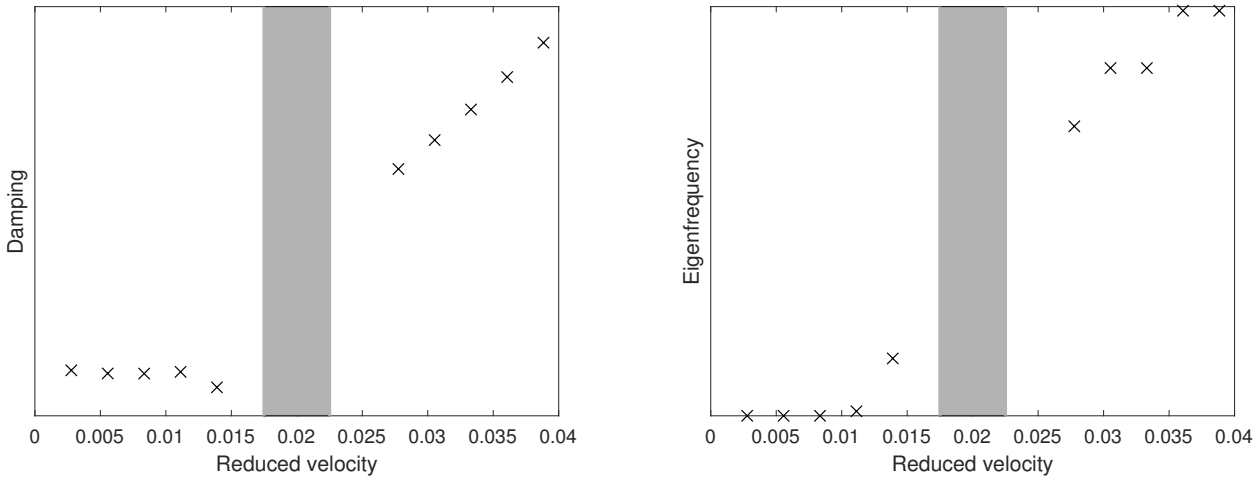

(a) Damping (b) Eigenfrequencies

Figure 6: Numerical simulation of damping and eigenfrequency across lock-in

4.3. Damping and Eigenfrequency

Figure 6 shows the damping and natural frequency of the Francis-99 hydrofoil. The x-axis shows the reduced velocity rather than the absolute velocity, due to the 2D representation of the foil. The scale on the y-axis is purposely omitted as the changes are fairly small and should not be compared with figure 1 in terms of absolute values, again due to the 2D representation, however the relative change is clear. The shaded areas represent the "lock-in" area where the change in characteristics changed in the experiments.

Comparing figure 6 to figure 1 it is clear that similar trends are seen. The change in damping across the "lock-in" is simulated before, but the fact that it is observed here as well verifies the methods used. More interesting is the figure showing the eigenfrequencies. Similar as for the damping, a clear change is observed when crossing the "lock-in" region. Such a shift would be impossible to obtain in a one-way coupled simulation, as the vibration frequency would be an input to the simulation, see i.e. [5].

The primary goal of the paper is to be able to simulate the shift in damping and eigenfrequency seen in the experiments. This was done in this section. Equally important is to understand *why* such phenomena occur. The following section will try to use one of the inherent advantages in the presented two-way procedure, the ability to separate the different terms in the second order oscillatory system, and track them over time.

If we start with the second order equation for structural oscillating motion, eq. 1, we can label the terms as *inertial, damping, restoring* and *external forcing*.

$$\overbrace{M\ddot{u}}^{\text{inertial forces}} + \overbrace{C\dot{u}}^{\text{damping forces}} + \overbrace{Ku}^{\text{restoring forces}} = \overbrace{F}^{\text{external forces}} \tag{15}$$

An observation; the structural damping in all simulations have been set to zero, yet damping is still observed. However, if the external forcing is also set to zero, as in section 4.1 where the discretization schemes was tested, there was no damping at all. This indicates that the damping originates in the external forcing. The next question is how.

One hypothesis is that the external force can have a phase shift relative to the structural deformation. If the force has such a phase shift, it can be decomposed into the different order

derivatives of the structural motion, $u, \dot{u}$. An equivalent or additional damping can then be found as the $\dot{u}$ component. This is a normal way of looking at the damping, see i.e. [5], as only the velocity-proportional term in eq. 1 is energy dissipative.

Assume that the deflection can be expressed as $u = a_1 sin(\omega t)$ and the forcing on the blade $F = a_F sin(\omega t + \phi)$. This means that the two are similar in shape and frequency, but separated by a phase shift. Now assume that the forcing can be decomposed into two terms;

$$a_F sin(\omega t + \phi) = a_u sin(\omega t) + a_{\dot{u}} cos(\omega t) \tag{16}$$

one term following the structural motion u, and one term following its derivative $\dot{u}$. This decomposition was done in MATLAB by solving a set of coupled equations for different phase shifts on a generic sinusoidal force. Figure 7 shows how the amplitudes of the decomposition changes with the phase shift. On closer inspection we see that the amplitude of the u-term follows the relation $a_u = cos(\phi)$, and the amplitude of the $\dot{u}$-term follows the relation $a_{\dot{u}} = sin(\phi)$. For small values of ϕ, $sin(\phi)$ is linear. This might explain why the damping is linearly increasing after lock-in, if the phase shift is also linearly increasing. This representation will not however, explain why the eigenfrequency increases, as figure 7a shows a strictly decreasing u-component of the force, going away from the lock-in region.

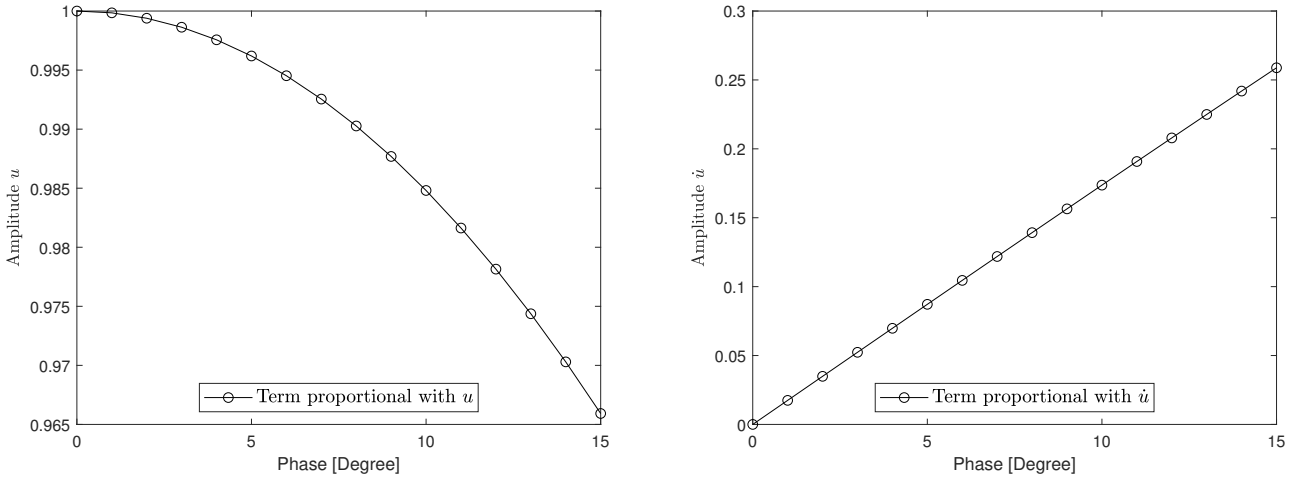

(a) Force decomposition in u-direction

(b) Force decomposition in $\dot{u}$-direction

Figure 7: Force decomposition

In fact, if we insert the "damping" from figure 7b into the classical formula for damped eigenfrequency, $f_d = f_n \cdot \sqrt{1 - \xi^2}$ we get exactly figure 7a. Additional information is therefore needed to separate the eigenfrequency component of the force.

From classical vibration we have that the eigenfrequency can be defined as $\omega_n = \sqrt{k/m}$, proportional to the stiffness and inversely proportional to the mass. Note as well that the above decomposition of the force does not separate between the u and $\ddot{u}$ components, as the two are the negative of each other (180° phase). This means that the u-component above really contains information regarding both. Or in other words, even if the sum is reduced, the ratio $r = k/m$ may not do so. An increase in this ratio would in theory increase the eigenfrequency. The next section will try to split the u-component into an acceleration and stiffness component.

Here we will use the inherent advantage of the two-way approach, the possibility to track the different forcing terms. Let us again start with the second order equation for structural

oscillating motion, with damping set to zero. If one during the derivation of equation 10 keeps the different forcing terms separated, we get discretized terms representing the inertial, restoring and external forces:

$$\overbrace{2(\frac{v_{i,k+1}-v_{i,k}}{\Delta t})}^{\text{inertial forces}}+\overbrace{\omega^2(q_{i,k+1}+q_{i,k})}^{\text{restoring forces}}=\overbrace{(f_{i,k+1}+f_{i,k})}^{\text{external forces}} \tag{17}$$

These terms, and their ratio can be tracked throughout the simulation as a way of quantifying the shift in eigenfrequency.

Figure 8a shows the approximate phase shift of the external forces with respect to the structural deformation. The phase shift is manually extracted from a time-series of the force and deflection, and will therefore be somewhat uncertain, however there seems to be an increasing trend across the lock-in region, although not as clear as in figure 6a.

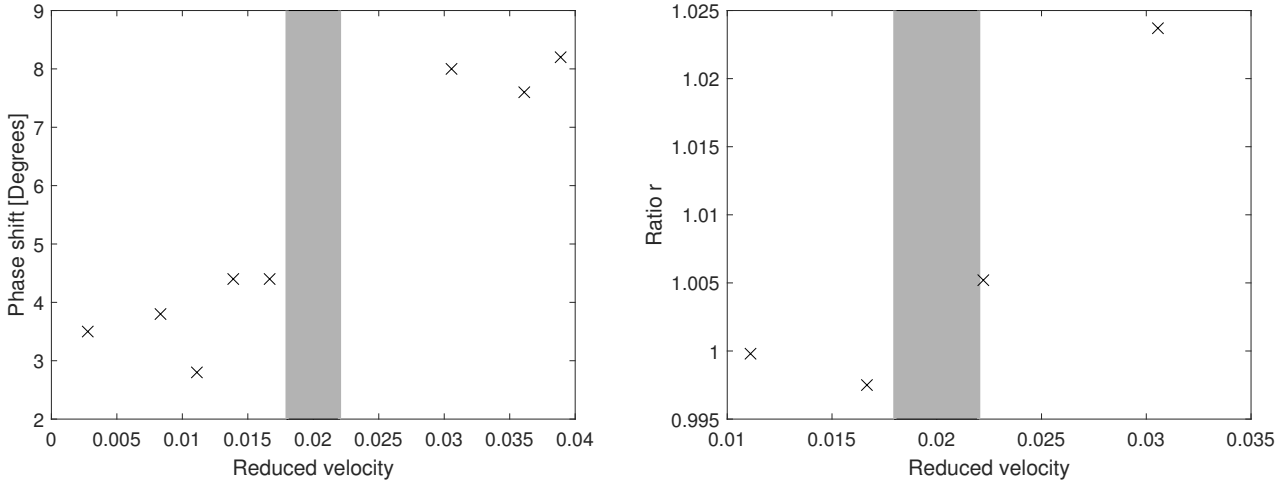

(a) Phase shift across lock-in

(b) r-ratio across lock-in

Figure 8: Analysis of phase shift between force and deflection (left), and ratio between restoring and inertial forces (right)

Figure 8b shows the approximate ratio between the restoring and inertial forces for the different flow velocities. Interestingly there is a change in this ratio across the lock-in region. It is dangerous to draw conclusions based on such a limited number of data points, however it seems like the r-ratio is about 1 before lock-in, but increases a couple of percent after. As discussed above, this change might be a reason for the added stiffness effect seen across the lock-in region.

4.4. Future work

In this paper, a modal decomposition-based model order reduction method was used. Some limitations apply, namely symmetric matrices such that a diagonal system can be created. This is then solvable inside CFX as simple expression evaluations. If a more sophisticated model order reduction technique was used, i.e. a Krylov based model, used on a similar geometry in [18], then this would allow for inclusion of phenomena such as gyroscopic effects, arbitrary damping and more. The simulation time would be the same, but as the reduced system is no longer simple evaluations, it would have to be solved by i.e. a Fortran script.

5. Conclusion

The hydrodynamic damping of a hydrofoil changes significantly across the lock-in region. The same is true for the eigenfrequency, there is actually a stiffening effect observed in experiments when the flow velocity is increased. Both effects are successfully simulated in this paper using a quasi-two-way FSI approach.

The hydrodynamic damping is approximately constant before the lock-in region and linearly increasing after, something shown numerically and experimentally earlier. This behaviour may be explained by the fact that the fluid load on the foil changes its phase relative to the foil, and thus dissipates more energy. The simulation of the added stiffness is new, and may be explained by tracking the inertial and restoring forces on the hydrofoil during the simulations. The ratio of the two is non-constant, and can be the reason for the changed behaviour.

Even though the test geometry in this case was fairly simple, the modal decomposition based two-way approach is shown to provide a great way of adding a layer of information to the simulations. Especially cases where there is a risk of significant fluid structure interaction could easily be investigated using this approach.

Acknowledgement

This work was done in the HiFrancis project, supported by the Norwegian Research Council and the Hydropower industry in Norway.

References

[1] Francis-99 research project `https://www.ntnu.edu/nvks/francis-99` accessed: 2019-03-12
[2] Bergan C W, Solemslie B W, Østby P and Dahlhaug O G 2018 *International Journal of Fluid Machinery and Systems* **11** 146–153
[3] Dörfler P, Sick M and Coutu A 2012 *Flow-induced pulsation and vibration in hydroelectric machinery: engineers guidebook for planning, design and troubleshooting* (Springer Science & Business Media)
[4] Bergan C W, Tengs E O, Solemslie B W and Dahlhaug O G 2019 *IOP Conference Series: Earth and Environmental Science* **240** 062008
[5] Tengs E O, Bergan C W, Jakobsen K R and Storli P T 2019 *IOP Conference Series: Earth and Environmental Science* **240** 062002
[6] Craig R R and Kurdila A J 2006 *Fundamentals of structural dynamics* (John Wiley & Sons)
[7] Clough Ray W and Joseph P 1995 *Computers & Structures, Inc*
[8] Zienkiewicz O C, Taylor R L and Zhu J Z 2005 *The finite element method: its basis and fundamentals* (Elsevier)
[9] Ansys® mechanical apdl, release 19.3, command reference, exprofile, ansys, inc.
[10] Ferziger J H and Peric M 2012 *Computational methods for fluid dynamics* (Springer Science & Business Media)
[11] Bergan C W, Tengs E, Solemslie B W and Dahlhaug O G 2019 Damping measurements on a multi-blade cascade with multiple degrees of freedom *Journal of Physics: Conference Series* (Accepted for publication)
[12] Kundu P K, Cohen I M and Dowling D 2008 Fluid mechanics 4th
[13] Gabbai R and Benaroya H 2005 *Journal of Sound and Vibration* **282** 575–616
[14] Bearman P W 1984 *Annual review of fluid mechanics* **16** 195–222
[15] Brekke H 1994 A review on oscillatory problems in francis turbines and simulation of unsteady flow in conduit systems *Proceedings of the 17th IAHR Symposium, Beijing, China* pp 15–19
[16] Sagmo K F, Tengs E O, Bergan C W and Storli P T 2019 *IOP Conference Series: Earth and Environmental Science* **240** 062006
[17] Coutu A, Seeley C, Monette C, Nennemann B and Marmont H 2012 Damping measurements in flowing water *IOP Conference Series: Earth and Environmental Science* vol 15 (IOP Publishing) p 062060
[18] Tengs E, Charrassier F, Holst M and Storli P T 2019 *International Journal of Applied Mechanics and Engineering* **24** 131–142